The pattern of retinal ganglion cell dysfunction in Leber hereditary optic neuropathy

Majander A.[1,2,3], Robson A.G.[2], João C.[1], Holder G.E.[1,2], Chinnery P.F.[4,5], Moore A.T.[1,2,6], Votruba M.[7], Stockman A.[1]*, Yu-Wai-Man P.[1,2,5,8]*

[1]UCL Institute of Ophthalmology

[2]Moorfields Eye Hospital, London

[3]Department of Ophthalmology, Helsinki University Hospital, and University of Helsinki, Helsinki

[4]MRC-Mitochondrial Biology Unit, Cambridge Biomedical Campus, Cambridge, CB2 0XY, UK

[5]Department of Clinical Neurosciences, Cambridge Biomedical Campus, University of Cambridge, Cambridge, UK

[6]Ophthalmology Department, UCSF School of Medicine, San Francisco, CA

[7]School of Optometry and Vision Sciences, Cardiff University Cardiff, and Cardiff Eye Unit, University Hospital Wales, Cardiff

[8]Wellcome Trust Centre for Mitochondrial Research, Newcastle University and Newcastle Eye Centre, Royal Victoria Infirmary, Newcastle upon Tyne

*Joint senior authors

Authors:

Andrew Stockman

 UCL Institute of Ophthalmology, London, UK

Anna Majander

 UCL Institute of Ophthalmology and Moorfields Eye Hospital, London, UK, and Department

 of Ophthalmology, University of Helsinki, and Helsinki University Hospital, Helsinki, Finland

Anthony G. Robson

 UCL Institute of Ophthalmology and Moorfields Eye Hospital, London, UK

Anthony T. Moore

 UCL Institute of Ophthalmology and Moorfields Eye Hospital, London, UK, and

 Ophthalmology Department, UCSF School of Medicine, San Francisco, CA

Catarina João

 UCL Institute of Ophthalmology, London, UK

33   Graham E. Holder

34   UCL Institute of Ophthalmology and Moorfields Eye Hospital, London, UK

35   Marcela Votruba

36   School of Optometry and Vision Sciences, Cardiff University Cardiff, and Cardiff Eye Unit,

37   University Hospital Wales, Cardiff, UK

38   Patrick F. Chinnery

39   MRC-Mitochondrial Biology Unit, Cambridge Biomedical Campus, Cambridge, CB2 0XY, UK,

40   and Department of Clinical Neurosciences, Cambridge Biomedical Campus, University of

41   Cambridge, Cambridge, CB2 0QQ, UK

42   Patrick Yu-Wai-Man

43   UCL Institute of Ophthalmology and Moorfields Eye Hospital, London, UK and Wellcome

44   Trust Centre for Mitochondrial Research, Newcastle University and Newcastle Eye Centre,

45   Royal Victoria Infirmary, Newcastle upon Tyne, and Department of Clinical Neurosciences,

46   Cambridge Biomedical Campus, University of Cambridge, Cambridge, UK

47

48   **Corresponding Authors:**

49   Anna Majander or Patrick Yu-Wai-Man. E-mails: anna.majander@hus.fi or

50   Patrick.Yu-Wai-Man@ncl.ac.uk

51

64   **Word count: 6938**

65

69

70

Abstract

72 Leber inherited optic neuropathy (LHON) is characterized by subacute bilateral loss of central vision

73 due to dysfunction and loss of retinal ganglion cells (RGCs). Comprehensive visual

74 electrophysiological investigations (including pattern reversal visual evoked potentials, pattern

75 electroretinography and the photopic negative response) performed on 13 patients with acute and

76 chronic LHON indicate early impairment of RGC cell body function and severe axonal dysfunction.

77 Temporal, spatial and chromatic psychophysical tests performed on 7 patients with acute LHON and

78 4 patients with chronic LHON suggest severe involvement or loss of the midget, parasol and

79 bistratified RGCs associated with all three principal visual pathways.

80

81 Word count: 100

82
83
84

85

86
87

88

1. Introduction

Leber hereditary optic neuropathy (LHON) (OMIM 535000) is a primary mitochondrial DNA (mtDNA) disorder that presents with bilateral subacute loss of central vision (Nikoskelainen et al., 1996; Yu-Wai-Man and Chinnery, 2000; Yu-Wai-Man et al., 2014). The majority of patients harbour one of three common mtDNA mutations (m.3460G>A in *MTND1*, m.11778G>A in *MTND4*and m.14484T>C in *MTND6*) that affect complex I subunits of the mitochondrial respiratory chain (Mackey et al., 1995). Despite the universal cellular role of mitochondria, retinal ganglion cells (RGCs) within the papillomacular bundle are particularly particularly severely affected accounting for the characteristic dense central or caecocentral scotoma in this disorder. Although the underlying pathological process is still not fully defined, this tissue specificity has been ascribed to an increased vulnerability of RGCs to both disturbed mitochondrial energy metabolism and the increased formation of reactive oxygen species (Carelli et al., 2004a; Lin et al., 2012; Sadun et al., 2000; Levin 2015; Sadun et al., 2015). LHON shows maternal inheritance, but there is variable disease penetrance and a marked sex bias with about 50% of male carriers losing vision during their lifetime compared with about 10% of female carriers (Mackey et al., 1995).

The histopathological observation of loss of the small calibre axons that constitute the papillomacular bundle was originally observed on histopathological sections of post mortem optic nerve samples obtained several decades after disease onset (Sadun et al., 1994; Kerrison et al., 1995; Sadun et al., 2000). More recently, *in vivo* studies involving high-resolution optical coherence tomography (OCT) have revealed a major loss of the temporal peripapillary nerve fiber (RNFL) and macular RGC layers within 3 months of disease onset. Interestingly, pathological thinning within the macular RGC layer was an early sign that was already apparent in the presymptomatic phase (Barboni et al., 2005; Barboni et al., 2010; Akiyama et al., 2013; Zhang et al., 2014; Mizoguchi et al., 2015; Balducci et al., 2015). Following disease conversion, swelling of the peripapillary RNFL spreads

113   circumferentially from the inferotemporal segment of the optic disc to involve the remaining

114   quadrants, before RNFL atrophy becomes established within 3-9 months after the onset of visual

115   loss. Hyperemia and fluctuating mild swelling of the prepapillary RNFL can also be seen in unaffected

116   LHON carriers without visual loss or progression to full disease conversion (Nikoskelainen et al.,

117   1982).

118   The function of the papillomacular bundle may be assessed objectively using pattern

119   reversal visual evoked potentials (PR-VEP) and pattern electroretinography (PERG). Reported PR-

120   VEP abnormalities in LHON are consistently severe, but the utility of the PERG in LHON is more

121   controversial and there are conflicting reports in the literature regarding the timing of responses and

122   the sequence of losses (Nikoskelainen et al., 1977; Hrynchak and Spafford, 1994; Mashima et al.,

123   1997; Sharkawi et al., 2012; Ziccardi et al., 2013; Ziccardi et al., 2015; Jarc-Vidmar et al., 2015). The

124   full-field photopic negative response (PhNR) has been used to assess generalised RGC function in

125   glaucoma and other acquired optic neuropathies (Machida, 2012; Morny et al., 2015), but there are

126   no published studies of PhNR in LHON. The applicability of PhNR as a potential objective functional

127   index of RGC function in LHON therefore warrants further investigation.

128   RGCs are classified into the three major subtypes of RGCs, namely midget, parasol and small

129   bistratified ganglion cells, which are thought to contribute to the parvocellular, magnocellular and

130   koniocellular pathways, respectively. These distinct RGC populations and their associated pathways

131   can be tested by modifying standard psychophysical measures. In general, the processing of high

132   spatial frequency information has been linked with the parvocellular pathway whereas high

133   temporal frequency information is thought to be integrated by the magnocellular pathway. Red-

134   green processing and blue-yellow processing have been linked with the parvocellular and

135   koniocellular pathways, respectively. Parallel processing in the retina and visual pathways have been

136   the subject of several recent comprehensive reviews (e.g., Dowling, 1987; Wässle and Boycott, 1991;

137   Rodieck, 1998; Lennie and Movshon, 2005; Lee, Martin and Grünert, 2010; Dacey, Crook, and

138   Packer, 2014).

139   LHON is thought to mainly affect midget RGCs, which have the smallest calibre axons and

140   are the predominant subtype within the papillomacular bundle, mediating visual information

141   including high spatial frequencies and red-green chromaticity (Sadun et al., 1994; Hrynchak and

142   Spafford, 1994; Kerrison et al., 1995; Sadun et al., 2000). In contrast, another melanopsin-expressing

143   RGC subtype appears relatively preserved and this peculiarity likely accounts for the frequently

144   preserved pupillary light reflexes, even in severely affected LHON patients (Kawasaki et al., 2010; La

145   Morgia et al., 2010). One previous report indicated mild impairment of the magnocellular pathway in

146   unaffected LHON carriers (Gualtieri et al., 2008), but there are no robust data regarding the

147   involvement of the parasol and small bistratified RCG subtypes in LHON.

148   In this study, we investigated the pattern of RGC dysfunction in a well-phenotyped cohort of

149   LHON patients in both the acute and chronic phases of the disease by using a comprehensive visual

150   electrophysiological and psychophysical assessment protocol. Our aim was, firstly, to characterise

151   the electrophysiological responses to better define the phenotypic features of LHON and to establish

152   the most appropriate methods for monitoring RGC function and disease progression objectively.

153   Secondly, we used psychophysical tests of temporal, spatial and chromatic vision to investigate the

154   relative involvement of distinct RGC populations in the pathophysiology of LHON.

155

156

2. Methods

2.1 Subjects

This was a prospective case study of 12 affected patients (A1-A12) and 9 unaffected carriers (U1-U9) harboring one of the three common mtDNA LHON mutations (**Table 1**). In addition, retrospective visual electrophysiological data for 5 affected LHON patients (A13-A17) were retrieved from the hospital database of Moorfields Eye Hospital, London, UK. In total, there were 4 affected female and 13 affected male patients. Affected LHON patients and unaffected LHON carriers in our cohort underwent an ophthalmological examination that included the following investigations as indicated in Table 1: best corrected visual acuity (BCVA) assessment using the Early Treatment Diabetic Retinopathy Study (ETDRS) chart; slit lamp examination; automated Humphrey visual field perimetry (Program 30-2, Humphrey Visual Field Analyzer, Model 750, Humphrey Instruments, San Leonardo, CA); and optical coherence tomography (OCT) imaging of the macula and the optic nerve head (see details below).

The normal subjects for psychophysical tests were 15 individuals aged 17 to 78 years old at the time of testing with normal BCVA and normal color vision as assessed by standard color vision tests. Only 12 of the normal subjects had their L-cone temporal contrast sensitivities measured. Written informed consent was obtained from all subjects or their guardians. The study was approved by the local ethics committees at Moorfields Eye Hospital and University College London and it conformed to the standards of the Declaration of Helsinki.

176

177

178

179

Table 1. Clinical characteristics of the recruited LHON cohort and the timing of investigations in relation to disease onset.

Subjects	Age (y) Sex	Genotype	BCVA logMAR*		Visual field defect MD (dB)		Time from LHON onset at study (months)				
							OCT		Electro-physiology		Psycho-physics
			RE	LE	RE	LE	RE	LE	RE	LE	RE/LE
Affected LHON patients											
A1	42 M	m.11778G>A	1.4	1.5*	-32.26	-28.63*	15	15	16	16	9 LE
A2	18 M	m.11778G>A	1.6	1.5*	-32.07	-32.89*	NP		18	18	10 LE
A3	19 F	m.3460G>A	1.9*	1.9	-34.39*	-34.46	0.7	0	17	16	10 RE
A4	21 M	m.11778G>A	2.0	2.0*	-34.18	-33.79*	15	19	15	19	9 LE
A5	17 M	m.11778G>A	2.2*	2.28	-34.48*	-34.31	10	10	14	15	10 RE
A6	15 M	m.11778G>A	1.6*	1.7	-29.11*	-28.56	6	6	8	8	6 RE
A7	22 M	m.11778G>A	0.7	0.8*	-19.36	-15.10*	32	32	NP		36 LE
A8	33 M	m.11778G>A	2.1*	2.1	-33.30*	-33.23	34	28			34 RE
A9	24 M	m.14484T>C	1.3*	1.3	-12.01*	-12.63	20	23			23 RE
A10	51 F	m.11778G>A	1.6*	1.6	-24.23*	-27.51	40	40			40 RE
A11	23 M	m.11778G>A	1.8*	2.3	-32.11*	-29.76	4	5			4 RE
A12	50 F	m.11778G>A	1.9	1.9	-30.54	-29.86	6	0	10	3	NP
A13	22 M	m.11778G>A	0.8	1.0	NP		0	1	0	1	
A14	36 M	m.14484T>C	1.3	1.0			98	98	5	5	
A15	7 M	m.11778G>A	0.6	2.0			140	140	27	27	
A16	7 F	m.3460G>A	1.7	1.5			NP		2	2	
A17	59M	m.3700G>A	1.9	1.9					20	20	
Unaffected LHON carriers											
U1	44 F	m.11778G>A	0*	0	-10.83*	-18.08	P		NP		P
U2	46 M	m.11778G>A	0*	0	-2.57*	-2.42					
U3	52 F	m.3460G>A	0.1*	0	-0.97*	-1.43					
U4	47 F	m.11778G>A	-0.1*	-0.1	-3.51*	-3.17					
U5	50 F	m.14484T>C	0.1*	0	0.18*	0.26					
U6	50 F	m.11778G>A	-0.1*	0.1	-2.59*	-0.24					
U7	41 F	m.3460G>A	0*	0	0.06*	-0.99					
U8	60 F	m.3460G>A	-0.1*	0	1.11*	0.22					
U9	46 F	m.11778G>A	0*	0	-1.81*	-1.64					

Abbreviations: BCVA, best corrected visual acuity: DOA, dominant optic atrophy; F, female; LE, left eye; LHON, Leber hereditary optic atrophy; M, male; NP, not performed; P, performed; RE, right eye.

* BCVA and MD of the eye used for the monocular psychophysics tests are indicated by asterisks.

185

9

186

2.2 Optical coherence tomography (OCT) imaging

188 The Spectralis^TM platform (Heidelberg Engineering Ltd., Heidelberg, Germany) was used for SD-OCT

189 imaging of the macula and the optic nerve head. Automated segmentation and thickness analyses

190 were performed for perifoveal volumetric retinal B-scans using the Heidelberg Engineering

191 segmentation tool, included in the Spectralis Glaucoma Module software (version 6.0). Of the 10

192 retinal layers that were automatically defined and manually confirmed, the following thickness

193 values were recorded from the four sectors of the inner ring (between 1 to 3 mm diameter) of the

194 nine macular ETDRS subfields as described elsewhere (Majander et al., 2016): (i) retina, (ii) retinal

195 nerve fiber layer (RNFL), (iii) combined GCL and inner plexiform layer (IPL), (iv) inner nuclear layer

196 (INL), (v) outer plexiform layer (OPL), (vi) combined OPL and outer nuclear layer (ONL), and (v) inner

197 retina. The thickness of the outer retinal layers was calculated by subtracting the thickness of the

198 inner retinal layers from the total retinal thickness. Normative data was generated from SD-OCT

199 images of 48 healthy eyes of 48 subjects (Majander et al., 2016). For peripapillary RNFL

200 measurement a 3.5-mm-diameter circular scan centered on the optic disc was used and the data for

201 six sectors were collected.

202

2.3 Electrophysiology investigations

204 Twelve subjects underwent electrophysiological testing including pattern reversal and flash visual

205 evoked potential (PVEP; FVEP) and pattern electroretinography (PERG), incorporating the standards

206 of the International Society for Clinical Electrophysiology of Vision (ISCEV; Odom et al. 2010, Bach et

207 al. 2013). Pattern ERGs were recorded to a 0.8- degree check size using both a standard

208 checkerboard field (12 x 15 degrees) and additionally to a large field (24 x 30 degrees; LF PERG;

209 Lenassi et al., 2012). The full-field photopic negative response (PhNR) was additionally recorded in 7

210 cases using diffuse red flash stimulation (640nm) at 5 flash strengths (0.5, 1.0, 2.0, 5.0 and 10.0

211 cd.s.m^{-2}), superimposed on a blue background (450nm; 2.25 cd.m^{-2}). Gold foil electrodes were used

212 and the results compared to normative data.

213

214 **2.4   Psychophysical investigations**

215 **2.4.1   L- and S-cone Critical Flicker Fusion and L-cone temporal contrast sensitivity**

216 L- and S-cone temporal acuities (critical flicker fusion, CFF) and L-cone temporal contrast sensitivity

217 functions (TCSFs) were measured using a Maxwellian-view optical system described in more detail

218 elsewhere (Stockman et al., 2005 and 2014a). Predominantly L-cone or S-cone stimuli were used for

219 the CFF measurements. The L-cone stimulus was produced by flickering a 650-nm circular target of

220 4˚ visual angle in diameter superimposed in the center of a steady 481-nm circular background field

221 of 9˚ diameter. The background radiance was fixed at 8.3 $\log_{10}$ quanta s^{-1} deg^{-2} and the target

222 radiance was varied in steps from 6.5 to 10.5 $\log_{10}$ quanta s^{-1} deg^{-2}. The S-cone stimulus was

223 produced by flickering a 440-nm circular target also of 4˚ diameter superimposed in the center of a

224 620-nm circular background field of 9˚ diameter. The 620-nm background radiance was fixed at 8.3

225 $\log_{10}$ quanta s^{-1} deg^{-2} and the 440-nm target radiance was varied in steps from 6.5 to 10 $\log_{10}$ quanta

226 s^{-1} deg^{-2}.   The 650-nm target and 481-nm background were also used for the L-cone TCSF

227 measurements with the time-averaged mean radiance of the 650-nm target fixed at 10.6 $\log_{10}$

228 quanta s^{-1} deg^{-2}. Before each run the subjects were light-adapted to the background and target for at

229 least 2 minutes. The observers viewed the stimuli monocularly with their preferred eye (see Table 2)

230 and interacted with the computer by means of an 8-button keypad. Each experiment was repeated

231 2-3 times on the same day. The method of adjustment was used. In the CFF measurements,

232 observers varied the frequency of the 650 or 440-nm target, which was sinusoidally-flickering with a

233 contrast of 92%, to find the frequency at each target radiance at which the flicker until the flicker

234 just disappeared. In the TCSF measurements, observers varied the contrast of the sinusoidally-

11

235   flickering 650-nm target to establish the contrast at each target frequency at which the flicker

236   disappeared. Details of these measurements have been given elsewhere (Stockman et al., 2014a).

237

238   **2.4.2   Achromatic spatial contrast sensitivity function (SCSF)**

239   Achromatic spatial contrast sensitivity (SCSF) was measured as a function of spatial frequency. The

240   target stimuli were generated on a gamma-corrected Sony Trinitron monitor (Model GDM F520)

241   with a resolution of 1600 x 1200 pixels and produced at a frame rate of 85-Hz. The monitor was

242   driven by a DataPixx video processor (VPixx Technologies Inc., Saint-Bruno, QC, Canada). The full

243   screen subtended a visual angle of 39˚ x 29˚ at a test distance of 0.57 m. The experiments were

244   performed at a constant mean luminance of 44.57 cd/m^2 as measured by a ColorCal calibration

245   device (Cambridge Research Systems Ltd., Rochester, UK). The stimuli were horizontally-orientated

246   Gabor patterns with spatial frequencies ranging from 0.25 to 16 cycles per degree (cpd) and with a

247   spatial Gaussian window with a standard deviation of 6˚. The target was presented for 500 ms,

248   preceded and followed by 100 ms cosine-windowed onsets and offsets. The order of presentation

249   was from low to high spatial frequency. Thresholds were measured using a staircase procedure. ,

250   Observers indicated whether or not they could detect the spatial variation in the Gabor pattern

251   using a 2-button keypad.

252   Stimulus contrast was defined as $(L_{max} - L_{min})/(L_{max} + L_{min})$, where L_{max} and L_{min} are the

253   maximum and minimum luminances in the Gabor pattern, respectively. Contrast was adjusted

254   according to a one-up-one-down staircase procedure with a variable step-size. The step-size was 0.3

255     $\log_{10}$ units for the first five reversals (changes in the direction of the staircase), after which it was

256   reduced to 0.2 $\log_{10}$ units for two more reversals and then finally to 0.1 $\log_{10}$ unit for the last four

257   reversals. A single run required a total of 9 reversals, with the contrast "threshold" taken as the

258   average of the last six reversals. Contrast sensitivity is the reciprocal of the contrast threshold. The

259 SCSF measurements lasted approximately 20 minutes for each observer. The stimuli were viewed

260 binocularly with natural pupils and appropriate correction if needed.

261

262 **2.4.3   Chromatic discrimination**

263 Chromatic discrimination was tested using the so-called trivector test procedure implemented as

264 part of the Cambridge Color Test (CCT), v1.5, (Cambridge Research Systems Ltd., Rochester, UK). The

265 test was performed using a second gamma-corrected Sony FD Trinitron color monitor (Model GDM-

266 F500R) connected to a VSG 2/5 visual stimulus generator (Cambridge Research Systems, Rochester,

267 UK) with 800 by 600 pixel resolution. The CRT phosphors measured in CIE 1976 u', v' chromaticity

268 coordinates (or CIE 1931 x, y coordinates) using ColorCal photometer (Cambridge Research System)

269 were: red phosphor (R) u'=0.416; v'=0.522 (x=0.610, y=0.340); green phosphor (G) u'=0.117;

270 v'=0.559 (x=0.280, y=0.595); blue phosphor (B) u'=0.159; v'=0.177 (x=0.142, y=0.070). The visual

271 stimuli consisted of Landolt "C" targets that varied in orientation presented on a background of

272 neutral chromaticity (CIE 1976 coordinates u'= 0.1977, v'=0.4689). The background and the target

273 were made up of small disks of variable size and luminance (ten equal steps between 8.0 and 18.0

274 cd.m^2). The circles making up the Landolt C were varied in chromaticity to find the threshold for

275 correctly discriminating the orientation of the Landolt C. The chromaticity was varied separately

276 along the three color directions that are invisible to observers lacking L-, M- or S-cones; that is, the

277 protan, deutan and tritan vector directions, respectively.

278   The test conditions were modified for observers with reduced visual acuity. Instead of the

279 viewing distance being set so that the Landolt "C" opening subtended 1° of visual angle, the viewing

280 distance was reduced to 62.6 cm so that the opening subtended 5° of visual angle. Two (A7, A9) of

281 the 11 affected LHON carriers, and one patient A6 after spontaneous recovery, were able to perform

282 the CCT test at this viewing distance. Another 5 patients were able to perform the test at a viewing

283   distance of 5 to 10 cm that enabled recognition of the orientation of the gap despite their central

284   scotomatas. Thresholds were measured along the protan, deutan, and tritan confusion lines. The

285   upper limit for target saturation was increased to 1600×10^{-4} u'v' units and the number of steps

286   increased from 6 to 10 in order to maintain the standard unit difference between the steps. The

287   time allowed for each subject to respond was increased from the standard 8 s to 20 s. The test was

288   then run using a standard descending psychophysical staircase procedure with six reversals.

289   Observers were instructed to respond to the gap position (four-alternative forced choice) by means

290   of a 4-button keypad. The test was performed binocularly with appropriate near corrections if

291   needed. Six of the affected LHON carriers repeated the CCT test 6 to 12 months after their first visit.

292

293   **2.5   Statistical analyses**

294   Mann-Whitney *U* independent samples test was used for comparison of distribution of continuous

295   variables in LHON and normal observers. Spearman's rank correlation test was used for the analysis

296   of statistical dependence between the variables.

297

298   **3.   Results**

299

300   **3.1   The acute phase of LHON is characterised by rapid loss of RGCs**

301   Macular SD-OCT revealed selective loss of the GCL-IPL complex thickness (50% of the normal) within

302   the first few months of disease onset in LHON as shown in the supplementary **Table S1** and **Figure 1**.

303   This occurred in parallel with loss of the temporal peripapillary RNFL thickness (Spearman *rho*=0.628,

304   p=0.002), whereas progression of RNFL thinning in the nasal sectors was less steep. The INL was

305   slightly, but significantly thicker in the affected LHON carriers compared with controls or the

306   unaffected LHON carriers.

307

308

309
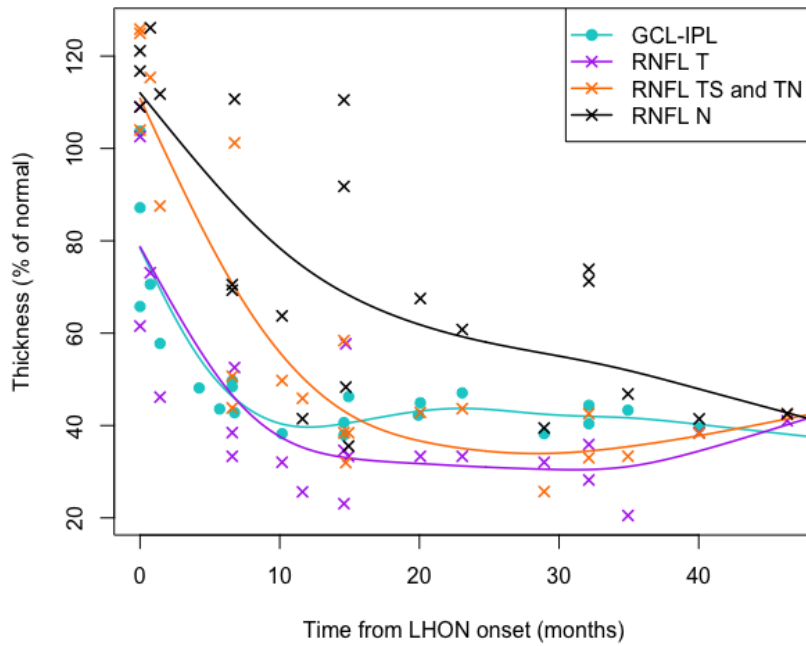
311 **Figure 1. Optical coherence tomography data.** Macular ganglion cell – inner plexiform layer complex
312 (GCL-IPL) and peripapillary retinal nerve fibre layer (RNFL) thicknesses of 22 eyes have been
313 presented as percentages of the normal mean and plotted as a function of time from LHON onset in
314 each eye. The data have been shown for temporal (T), nasal (N) and combined supero- and
315 inferotemporal (TS and TI) sectors of peripapillary RNFL. Generalized additive model (GAM) fits to
316 data are indicated by the colour coded lines.

317

318

319 **3.1   Visual electrophysiology: pattern responses were more severely affected than photopic**

320 **negative ERG responses**

15

321   The age of the patients at the time of electrophysiological testing ranged from 7.5 to 59.0 years

322   (mean = 26.6 years; SD = 16.7 years). The duration of symptoms ranged from 0 to 27 months (mean

323   12.5 months). Visual acuity was severely impaired in all cases (range = 1.3 logMAR to perception of

324   light). Characteristic electrophysiology waveforms for affected LHON carriers are shown in **Figure 2**.

325   Photopic negative responses were attenuated at all stimulus strengths (see corresponding plots in

326   Figure 2c and 2d; orange circles). Pattern reversal VEPs were undetectable and flash VEPs were

327   grossly abnormal. Pattern ERG P50 is of short peak time and the waveforms had a low N95:P50 ratio,

328   in keeping with severe optic nerve/retinal ganglion cell dysfunction bilaterally.

329

330

| Pattern VEP | Flash VEP | Standard PERG | Large field PERG |
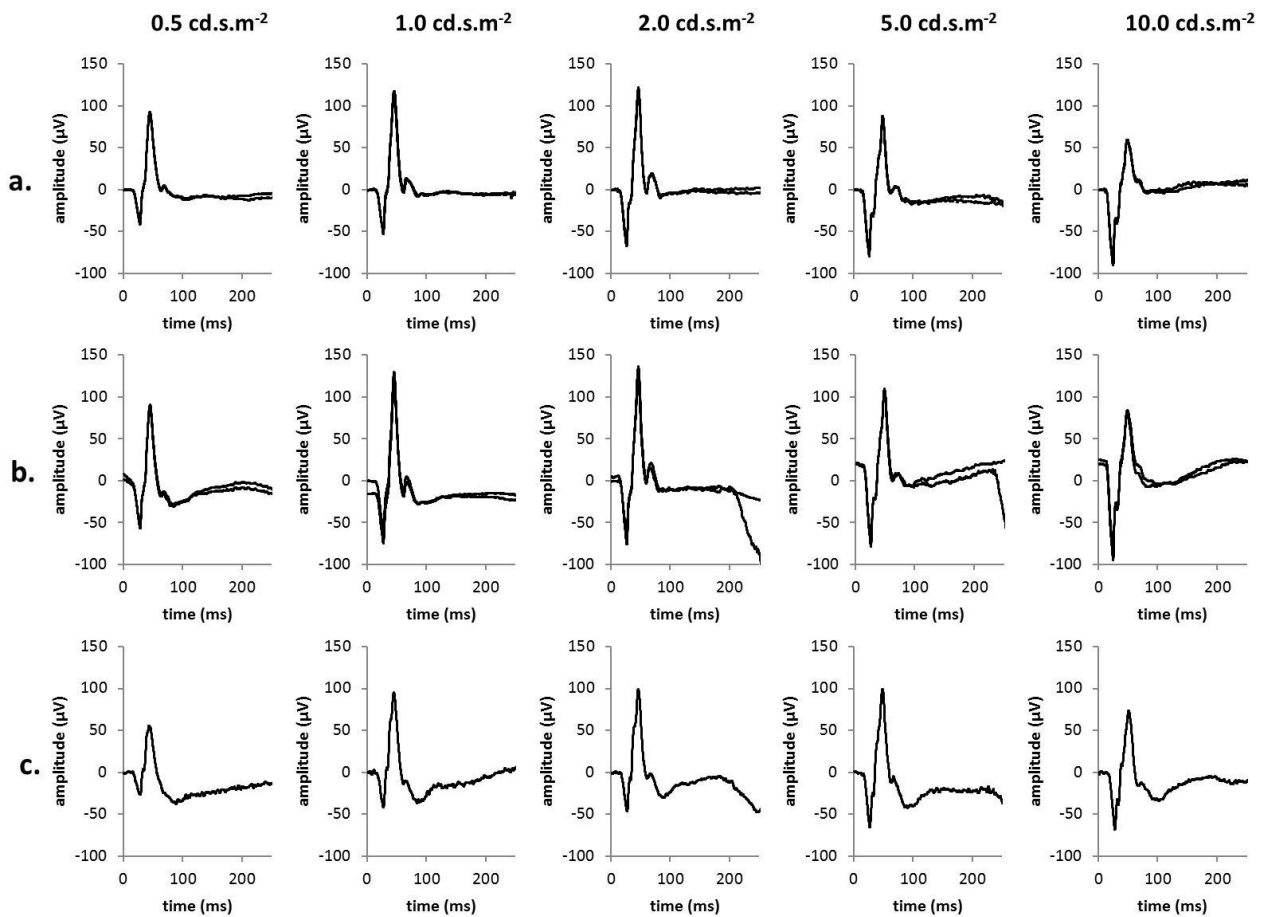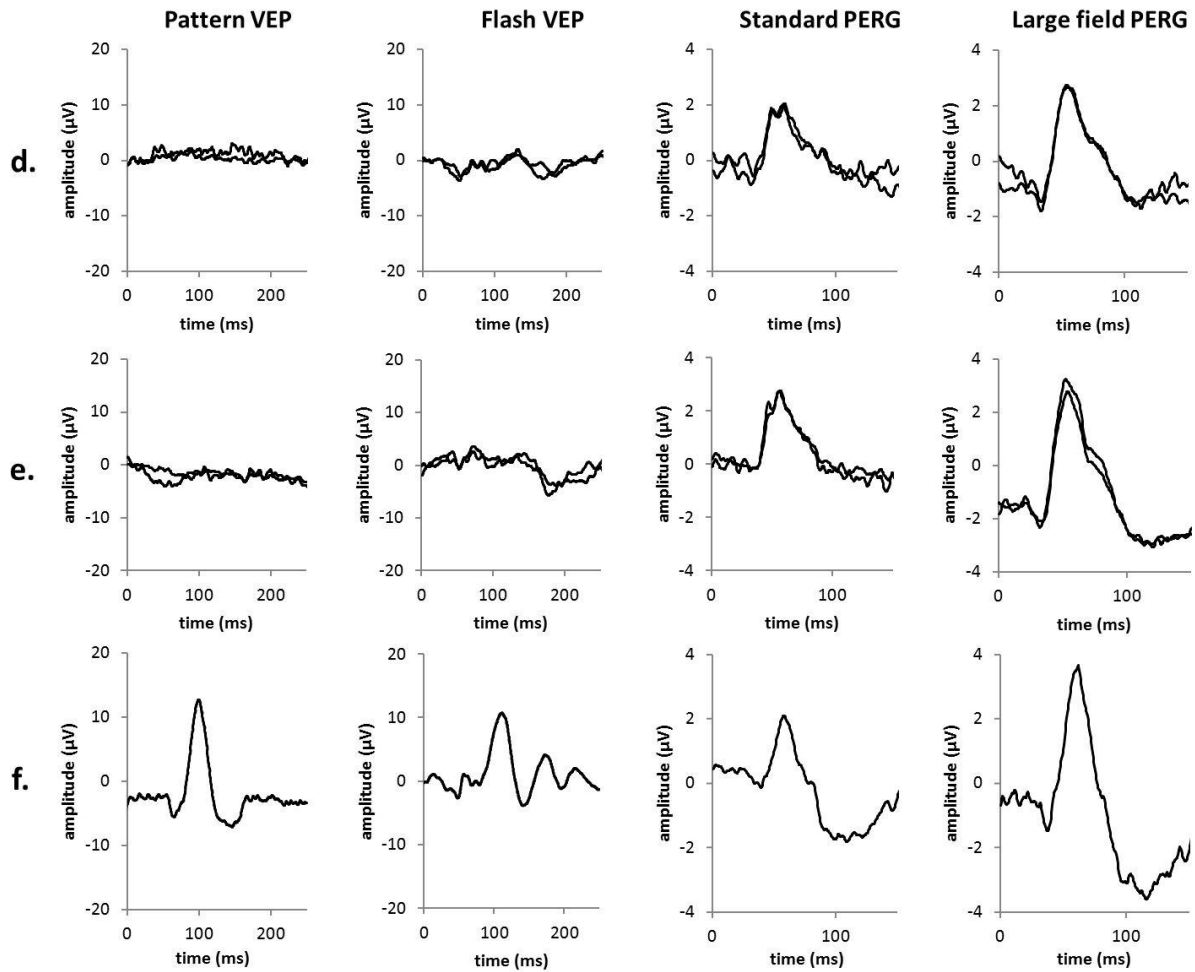
Figure 2. Photopic negative responses from the right (a) and left (b) eyes of a patient with LHON (A3). For comparison, representative normal recordings over a range of flash strengths (0.5-10.0 unit) have been provided (c). Pattern reversal VEPs, flash VEPs and pattern ERGs are shown for the right (d) and left (e) eyes of Patient A3 compared with representative normal recordings (f). The patient's recordings have been superimposed for all the parameters tested to demonstrate reproducibility.

Pattern reversal VEPs were undetectable in 20 of 24 eyes and were delayed in 4 eyes of 4 subjects with detectable responses (peak time 121-142ms; upper limit of normal 115ms); amplitudes in 2 of the eyes with a delayed VEP were within the normal range (>4µV). Flash VEPs were undetectable in 5 eyes of 3 subjects (all with undetectable pattern VEP), were delayed (P2> 140ms) in 5 eyes, and were present but subnormal (<5µV) in 20 eyes. Flash VEPs were normal in 3 eyes of 2 subjects including one of the youngest individuals (age 7.5 years). The severity of pattern and flash VEP abnormality did not significantly correlate either with age or duration of symptoms.

17

345   Pattern ERG P50 to a standard stimulus (field size 12˚ x 15˚) was of abnormally short peak

346   time (<45.5ms) in 19 of 21 eyes (**Figure 3a** PERG). P50 was of normal amplitude in most, mildly

347   subnormal (<2.0µV) in 4 eyes of 4 patients (1.5-1.9µV) and of borderline amplitude (2.0µV) in a

348   further 2 eyes (**Figure 3b** PERG); P50 was of shortened peak time in all 6 eyes with a borderline or

349   mildly subnormal amplitude. The N95:P50 amplitude ratio was subnormal (<1.1) in 17 of 19 eyes

350   (0.75-1.0) and at the lower limit of normal (ratio = 1.1) in a further 2 eyes (mean and median ratio of

351   all cases 1.0; SD 0.1; **Figure 3c** PERG). PERGs were technically poor in 5 eyes of 4 cases due to

352   variable fixation (N=1); pupil dilation (N=1) or physiological noise and those eyes were excluded from

353   analysis. PERG to a doubled stimulus field (24˚ x 30˚) were obtained in 11 patients including 4 eyes in

354   which the standard field PERG was excluded. Data were compared with a normative data set

355   obtained using the same large field stimulus. Sixteen of 22 eyes were of abnormally short peak time

356   (<46.5ms; **Figure 3d** PERG) and these included 4 patients with additional bilateral P50 reduction

357   (1.9µV-2.7µV; normal>3.9µV). The N95:P50 ratio was subnormal in 8, borderline in 10 and normal in

358   5 eyes (**Figure 3e** PERG). There was no significant correlation between pattern ERG parameters and

359   age or duration of symptoms.

360   International-standard full-field ERGs revealed no clinically significant abnormality in the 7

361   individuals tested. PhNRs were recorded from 14 eyes of 7 cases, including 5 individuals that did not

362   undergo standard full-field ERGs. The ratios of PhNR/b-wave ratios were within the normal range in

363   1 eye at all 5 flash intensities; in others the ratio was subnormal to one flash strength (N= 2 eyes),

364   two (N=3 eyes), three (N= 1 eye), four (N=4 eyes) or 5 flash strengths (N=3 eyes) (**Figure 4** PhNR).

365   The mean magnitude of reduction of subnormal responses was 13% (range 1.5-23%) compared with

366   the lower limit of normal. Forty percent of responses showed no abnormality (**Figure 4c and 4d**).

367

368
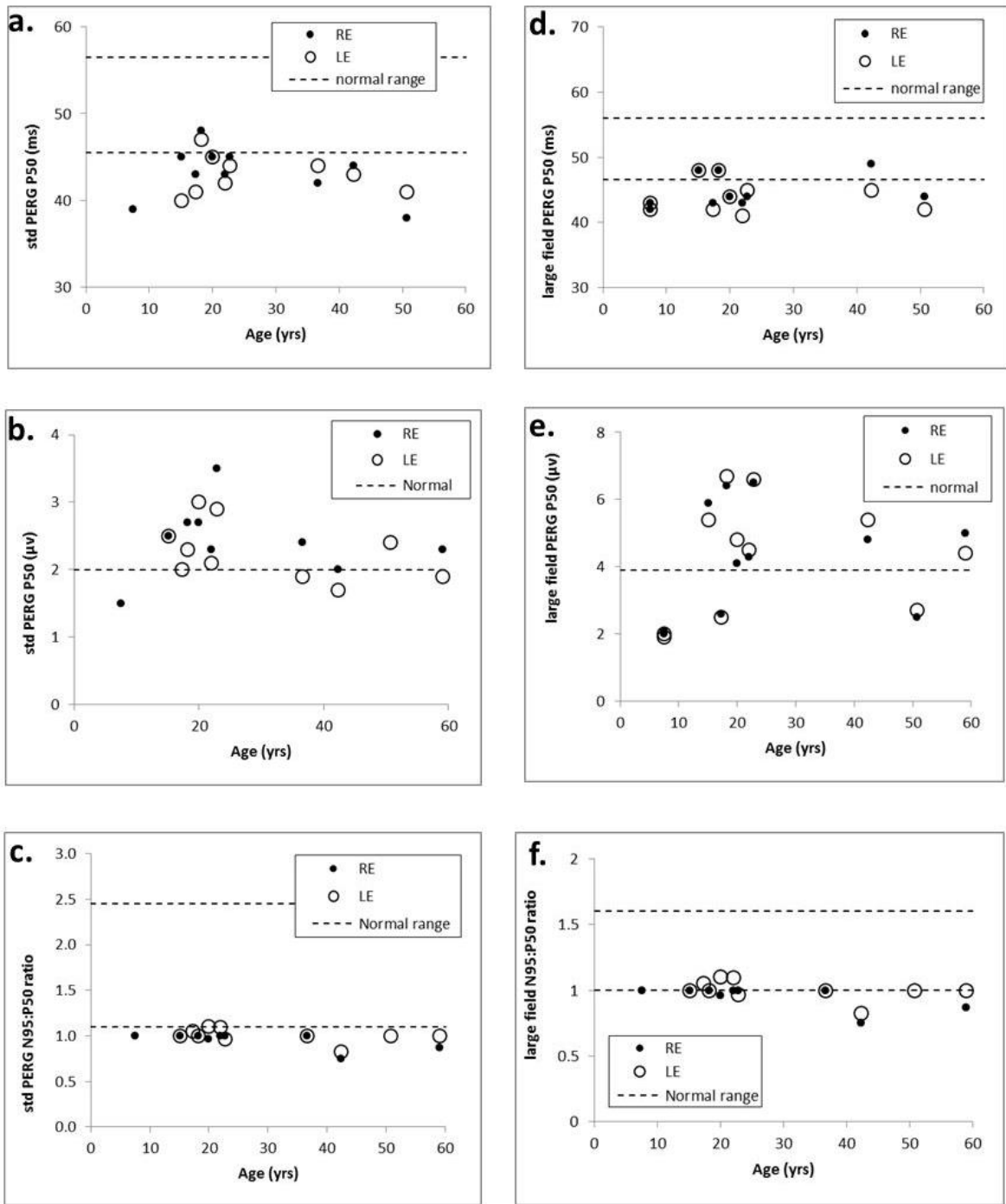
369

370 *Figure 3. Pattern ERG data*. *Pattern ERG parameters were obtained to a standard (12˚ x15˚; **a-c**) and*
371 *large (24 x 30 degrees; **d-f**) checkerboard stimulus field for right and left eyes (RE; LE). Broken lines*
372 *show the limits of normality defined as the minimum/maximum amplitude or peak time in a healthy*
373 *cohort of subjects +/- the reference interval (maximum normal value-minimum normal value).*
374 *Pattern ERG peak times and/or the N95:P50 ratio were abnormal in all the cases. Large field pattern*

ERG parameters were abnormal in most cases, including those in which PERG to the smaller field was excluded. The P50 amplitude of the pattern ERG was normal or near-normal in most cases, indicating good fixation despite of poor visual acuity.
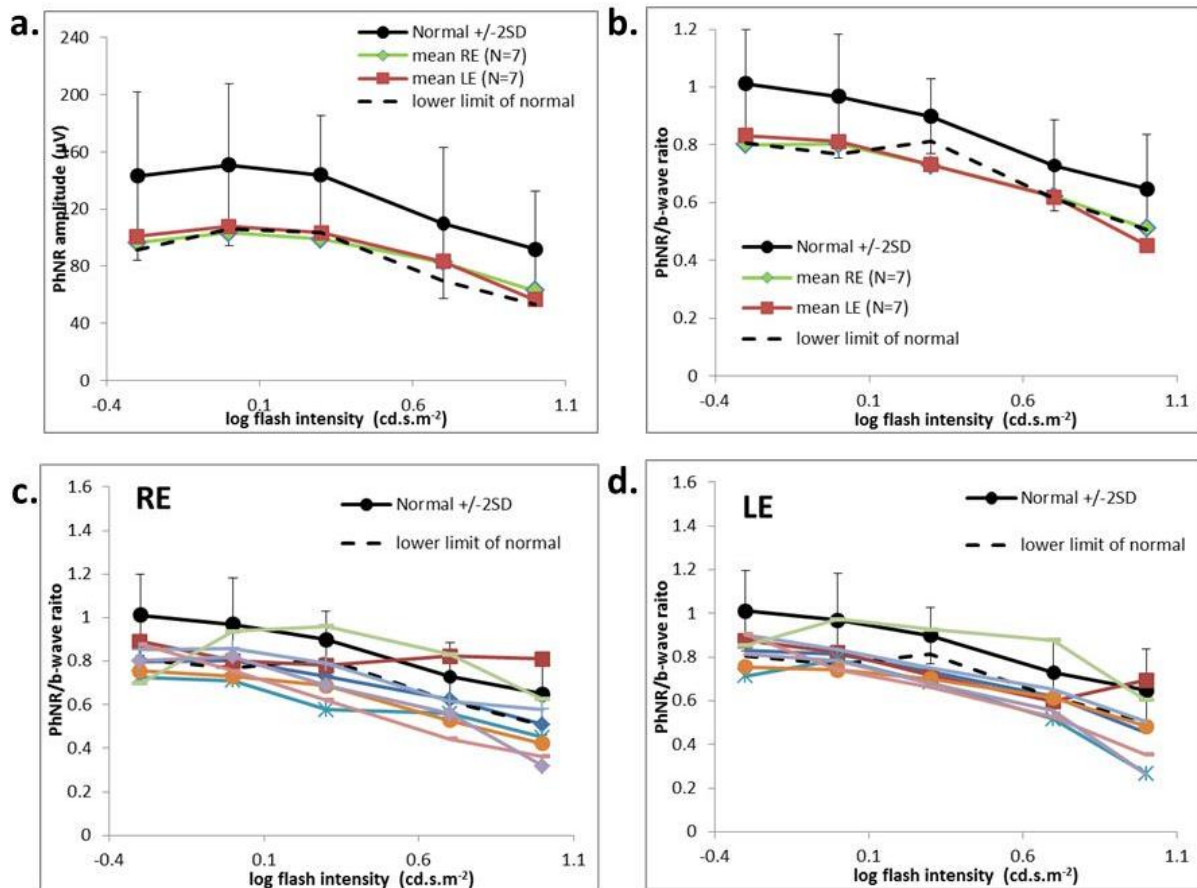
2 COLUMNS WIDTH

Figure 4. Photopic negative response (PhNR) data. *Mean photopic negative responses (**a**) and the mean PhNR/b-wave ratio (**b**) were recorded in 7 individuals with LHON and compared with normal values at 5 flash strengths. The solid line and error bars show the mean normal values and 2 standard deviations from the mean. Broken lines show the limits of normality defined as the minimum amplitude in the normal cohort minus the 5% of the reference interval (maximum normal value-minimum normal value). Ratios from each individual are shown for right (RE; **c**) and left (LE; **d**) eyes. Sixty percent of responses were just outside the limits of normality (see text for details).*

392

393

3.2 Visual Psychophysics

3.2.1 L-cone temporal functions were severely compromised in LHON

The data for L-cone cff (temporal acuity) are presented in **Figure 5** and are summarized in the supplementary **Table S2**. In the normal observers (grey triangles), flicker was first seen at a target radiance of 6.6 $\log_{10}$ quanta s^{-1} deg^{-2}. The cff then grew linearly with log radiance over about 3 $\log_{10}$ units with a slope of 9.2 Hz per $\log_{10}$ unit (see upper blue line in the lower panel) until reaching a plateau near 40 Hz (Stockman et al. 2014a). The linear relationship between cff and log radiance is known as the Ferry-Porter law (Ferry, 1892; Porter, 1902). Eight of the 11 affected LHON carriers were able to detect L-cone flicker, but the mean radiance of 9.6 $\log_{10}$ quanta s^{-1}deg^{-2} at which flicker was first seen was 30 times higher than that for normal observers (**Table S2**). Three patients could detect flicker only at the highest target radiances. LHON patients thus required higher radiances to detect flicker than normal subjects and their cffs showed severe losses reaching a mean plateau of only 12 Hz, 28 Hz less than normal subjects. The lowest radiance at which unaffected LHON carriers first detected flicker was slightly higher than that for normal subjects (**Table S2**). Three carriers (U2, U6, U9) had significantly shallower Ferry-Porter slopes than normal and only three carriers (U1, U4, U8) had cffs that reached the normal plateau level of 40 Hz. The majority of the LHON carriers showed some loss of cff. Patient A6 experienced spontaneous recovery of BCVA from 1.6 logMAR to 0.1 logMAR between 6 to 18 months after LHON onset. His cff improved, but only marginally (A6 F, yellow squares).

Figure 6 shows the L-cone temporal contrast sensitivity data. The mean L-cone TCSF for normal subjects peaks in sensitivity near 8 Hz and falls off in sensitivity at both low and high temporal frequencies (Stockman et al. 2014a and 2014b; Ripamonti et al. 2014). Only patients A3, A7 and A9 of the affected carriers were able to perform the test and showed a mean sensitivity loss of 1.0 $\log_{10}$ unit. Unaffected LHON carriers had normal L-cone temporal modulation sensitivities but were unable to make settings at the highest temporal frequencies, consistent with their lower cffs.
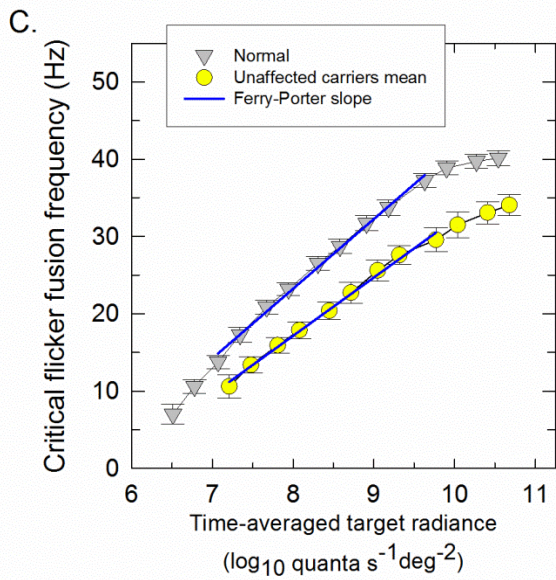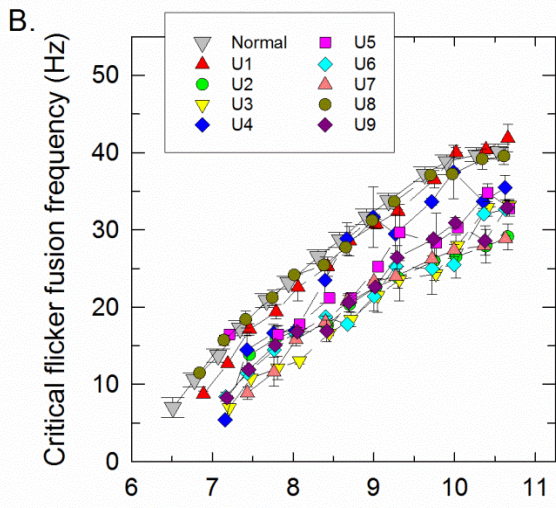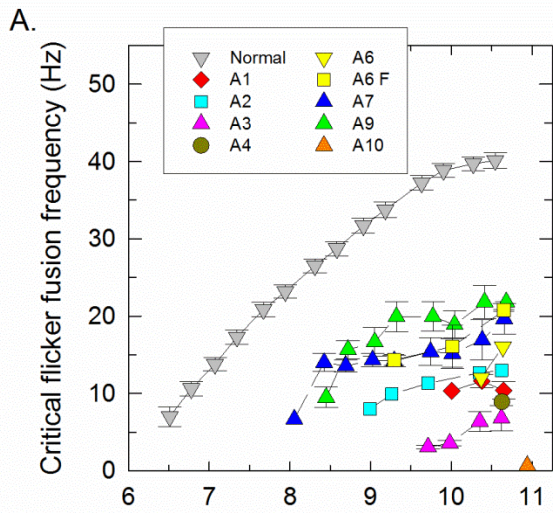
423 ***Figure 5. L-cone critical flicker fusion***. *L-cone critical flicker frequencies (cff) were measured on a*
424 *481–nm background of 8.26 $\log_{10}$ quanta $s^{-1}deg^{-2}$ and plotted as a function of the mean $\log_{10}$*
425 *radiance of a 650-nm flickering target for the affected **(A)** and unaffected **(B)** LHON carriers. The*
426 *mean cff data for 15 normal observers are represented by the grey triangles in all panels. The yellow*
427 *squares (A6 F) indicate follow-up data for Patient A6, which were obtained after spontaneous*
428 *recovery of best corrected visual acuity from 1.6 logMAR to 0.1 logMAR in the right eye. **(C)** Mean L-*
429 *cone cff data for all unaffected LHON carriers (yellow circles)were compared with the mean normal*
430 *data (grey triangles). The best-fitting Ferry-Porter slopes are indicated by the blue lines. The error*
431 *bars represent ± 1 SEM either between runs for the individual patients or between observers for the*
432 *mean data.*

433
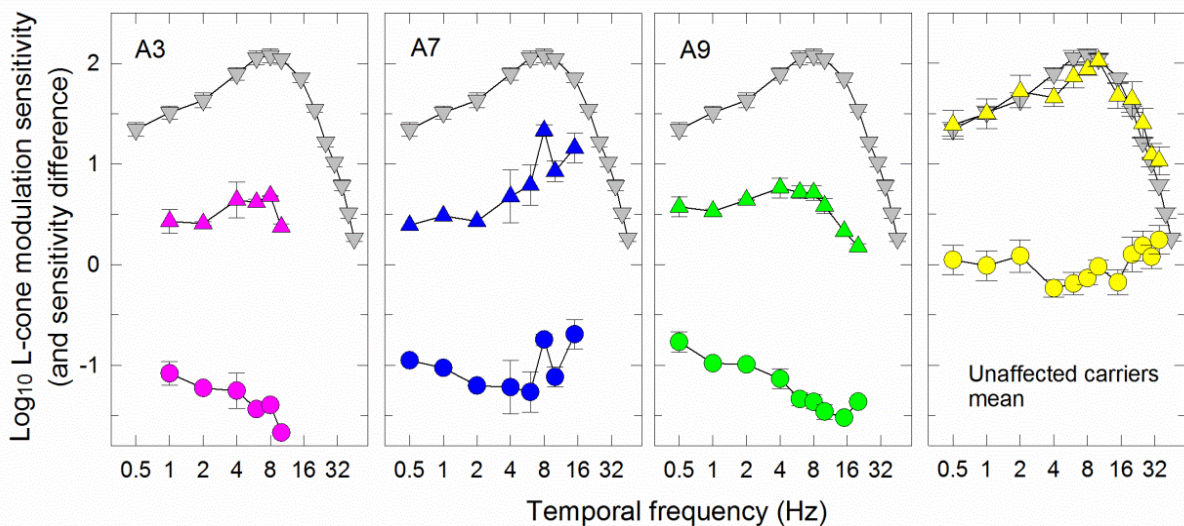
434

435 2 COLUMNS WIDTH

436 ***Figure 6. $\log_{10}$ L-cone temporal contrast sensitivity.*** *$\log_{10}$ L-cone TCSFs were measured using a*
437 *sinusoidally-modulated 650-nm target with a time-averaged mean radiance of 10.28 $\log_{10}$ quanta s^{-1}*
438 *deg^{-2} superimposed on a 481-nm background of 8.29 $\log_{10}$ quanta s^{-1} deg^{-2} plotted as a function*
439 *temporal frequency (logarithmic axis) for three affected LHON carriers (A3, A7, A9) (pink, blue and*
440 *green triangles, respectively) and for the mean of 9 unaffected LHON carriers (yellow triangles). The*
441 *mean TCSFs for 12 normal observers have been shown as grey triangles. The error bars represent ± 1*
442 *SEM either between runs for the individual patients or between subjects for the mean data. The*
443 *mean difference in log sensitivity between each affected or the mean of unaffected LHON carrier and*
444 *normal subjects are shown in the lower part of each panel (circles).*

445

446

3.2.2   S-cone temporal function was unmeasurable in most LHON patients and reduced in the unaffected m.3460G>A carriers

In the normal subjects, flicker was first seen at a target radiance of about 6.5 $\log_{10}$ quanta $s^{-1}deg^{-2}$.

Thereafter, the cff grows linearly with log radiance with a slope of 7.3 Hz per $\log_{10}$ unit, consistent

with the Ferry-Porter law, until reaching a plateau at 9.0 $\log_{10}$ quanta $s^{-1}deg^{-2}$ (see **Figure 7** and the

supplementary **Table S3**). The rise after 9.9 $\log_{10}$ quanta $s^{-1}deg^{-2}$ is due to M-cone intrusion - the M-

cones become more sensitive than S-cones at high radiances and thus mediate flicker detection

(Stockman et al. 1998 and 2014a).

Only two affected LHON carriers (A7, A9) were able to detect any 440-nm flicker, and all

showed severely impaired temporal acuity. S-cone cff was relatively normal for the unaffected

carriers of the m. 11778G>A and the m. 14484T>C mutations, who first saw flicker at 07.10±0.06

(mean±1 SEM) $\log_{10}$ quanta $s^{-1}deg^{-2}$, and exhibited a Ferry-Porter slope of 7.97±0.39 Hz per decade

(mean±1 SEM) and a cff plateau frequency of 22.94±0.57 Hz (mean±1 SEM). In contrast, S-cone cff

for the three carriers harboring the m.3460G>A mutation was compromised: those subjects first saw

flicker at a radiance of 8.06±0.51 $\log_{10}$ quanta $s^{-1}deg^{-2}$, and exhibited a shallow Ferry-Porter slope of

5.03±1.05 Hz per $\log_{10}$ unit, the cff reached a plateau frequency of 12.61±3.80 Hz. One carrier of the

three with the m.3460G>A mutation could detect flicker only at the highest radiances, but was

within normal limits for the tritan measurements in the CCT (see below).
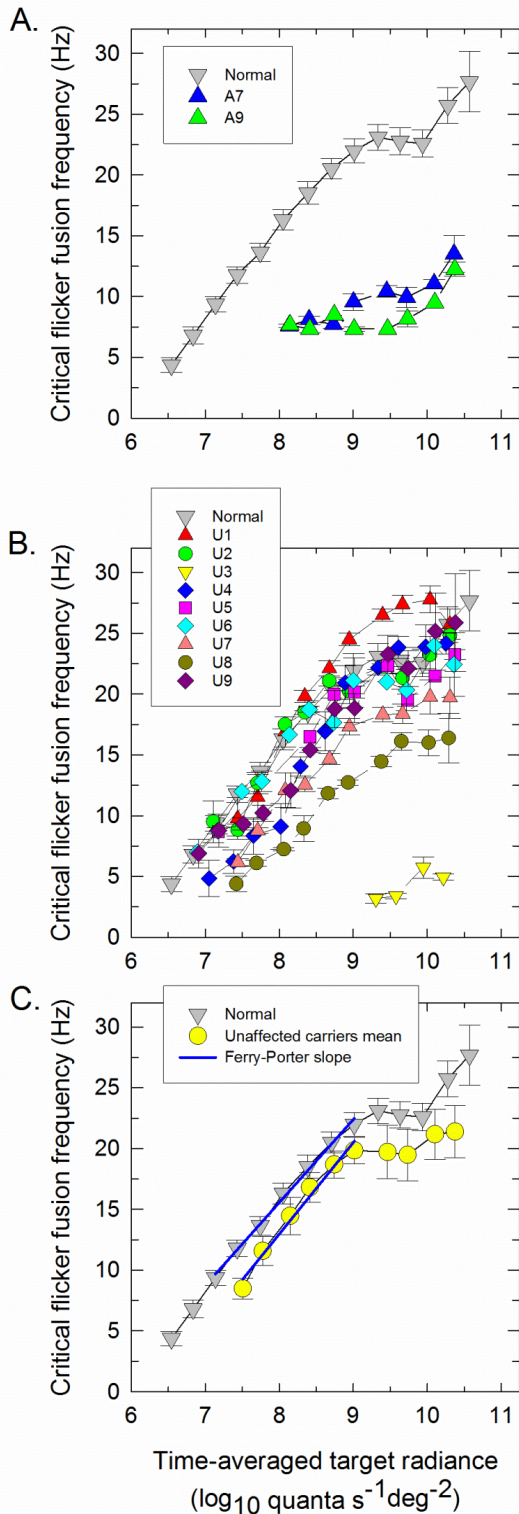
Figure 7. S-cone critical flicker frequencies (cff). This parameter was *measured on a a 9° 620 –nm background of 11.41 log$_{10}$ quanta s^{-1}deg^{-2} and plotted as a function of the time-averaged mean log$_{10}$ radiance of a 440-nm flickering target for each affected (**A**) and unaffected (**B**) LHON carrier (colored symbols). The mean cff data for 15 normal subjects are shown by the grey triangles in all panels. (**C**). Mean S-cone cff data for all unaffected LHON carriers (yellow circles) compared with the mean normal data (grey triangle). The best-fitting Ferry-Porter slopes are indicated by the blue lines (**C**). The error bars represent ± 1 SEM either between runs for the individual patients, or between subjects for the mean data.*

486

3.2.3 Achromatic spatial contrast sensitivity function (SCSF) was unmeasurable in most LHON

patients and mildly subnormal in the unaffected carriers

489 The mean achromatic spatial contrast sensitivity function for normal subjects is shown as inverted

490 grey triangles in each of the three panels of supplementary Figure S1. The function is band-pass in

491 shape peaking at 2 cpd and falling off in sensitivity at lower and higher spatial frequencies

492 characteristic of other SCSFs measured at moderate and high intensities (Robson, 1966; van Nes and

493 Bouman, 1967). Only two (A7 and A9) of the 11 affected LHON carriers could perform this test. Both

494 patients showed a loss of contrast sensitivity that increased with frequency. In the unaffected LHON

495 carriers, the achromatic SCSF was normal at the lowest spatial frequency but showed increasing loss

496 as spatial frequency increased.

497

3.2.4 Chromatic discrimination was severely affected in LHON

499 **Figure 8A** shows the vector lengths of the three confusion lines (protan, deutan, and tritan) of the

500 Cambridge Color Test in 10^{-4} *u'v'* units (the CIE 1976 *u'v'* color space). The longer the vector length

501 the more saturated the color had to be for the orientation of the gap in the Landolt C to be

502 discriminated. The maximum vector lengths were 1600 10^{-4} *u'v'* units (the CIE 1976 *u'v'* color space).

503 The vector lengths in the normal observers were comparable to those previously reported using

504 standard targets with 1 degree gaps: 45.1±1.0 for protan, 43.3±0.8 for deutan and 51.5±1.3 for tritan

505 in 10^{-4} *u'v'* units (the CIE 1976 *u'v'* color space) [mean±SEM] (Paramei and Oakley 2014). Altogether,

506 8 affected LHON carriers could discriminate the gap in the Landolt C, most viewed the CRT screen

507 from only 5 to 10 cm Their vector thresholds along the protan and the deutan axes on their first

508 tests were 25.8±2.6 (mean±SEM) and 25.4±2.8 times higher, respectively, than controls whereas

509 along the tritan axes the vectors were only 5.1±0.7 times higher. **Figure 8B** shows the vector lengths

510 of the successive tests made on six affected LHON carriers. Three affected carriers (A1, A3, A6),

511   initially studied 6 to 9 months after LHON onset, showed recovery of color discrimination, mainly

512   along protan and deutan axes. Chromatic discrimination in unaffected LHON carriers was only

513   marginally subnormal along all chromatic axes with high normal vector lengths. Affected observers

514   therefore show a general loss along all three axes.

517

518
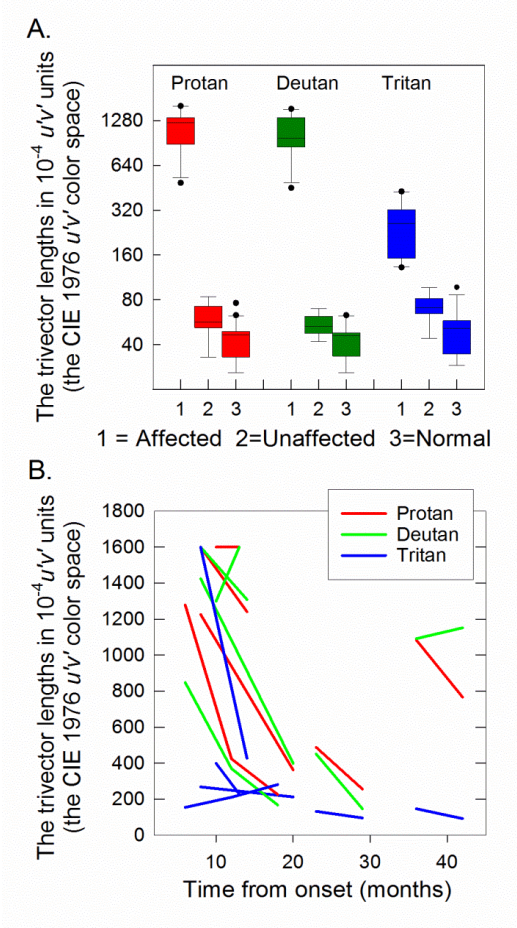
*Figure 8. The Trivector Cambridge color test. (A) Box plots of the logarithmic vector lengths along the protan, deutan and tritan confusion lines expressed in 10^{-4} u'v' units (defined by the CIE 1976 u'v' color space) for the affected (**1**, n=8) and unaffected (**2**, n=9) LHON carriers, and for normal observers (**3**, n=15), showing median, range, inter-quartile range and outliers for all groups. (B) Changes in the vector lengths along the protan, deutan and tritan confusion lines have been expressed as 10^{-4} u'v' units for successive measurements of 6 affected LHON carriers and plotted as a function of time from disease onset.*

515

534

535

4. Discussion

Our comprehensive electrophysiological and psychophysical study of patients with acute and chronic LHON highlights the marked extent of RGC dysfunction in this classical mitochondrial optic neuropathy.. Our study also indicates the utility of the standard transient pattern ERG technique in patients with LHON, with the recordings revealing severe central RGC dysfunction in all the patients tested, irrespective of visual acuity, age or the duration of symptoms. Detailed psychophysical data demonstrated loss of visual function in affected LHON carriers across a range of parameters, including achromatic spatial and L-cone temporal contrast sensitivity, L- and S-cone acuity, and chromatic discrimination. These findings are consistent with substantial losses of the principal RGC subtypes associated with each of the three major retinal pathways. Furthermore, with the exception of L-cone TCSF, unaffected LHON carriers also showed subclinical abnormalities in all the psychophysical measures that were evaluated.

A number of studies have reported abnormal cortical PR-VEPs responses in acute LHON, (Nikoskelainen et al., 1977; Hrynchak and Spafford, 1994; Mashima et al., 1997; Sharkawi et al., 2012; Ziccardi et al., 2013). Our PR-VEP results are consistent with these previous observations and the early involvement of the papillomacular bundle in this mitochondrial optic nerve disorder. The PERG reflects central retinal function and has two major components; the positive P50 and negative N95 (Holder, 1987). The N95 component arises in RGCs whereas approximately 30% of the P50 component originates in more anterior retinal structures (Holder, 1987, 2001; Ryan and Arden, 1988; Viswanathan et al., 2000). P50 is widely used to assess macular function whereas reduction in the N95:P50 ratio with preservation of P50 amplitude or shortening of P50 peak time suggests RGC dysfunction (Holder, 2001). However, reports of PERG findings in LHON have been contradictory (Sharkawi et al., 2012; Ziccardi et al., 2013; Jarc-Vidmar et al., 2015). Some studies of LHON have used surface electrodes and rapidly alternating stimuli to elicit steady-state PERG recordings (Lam et al., 2010; 2014) but the signal:noise ratio for surface recordings is lower than for corneal recordings and abnormal amplitude reduction does not distinguish macular from retinal ganglion cell

562   dysfunction. Our study found consistent PERG abnormalities with shortened P50 peak time and

563   reduced N95:P50 ratio in patients with acute LHON. Furthermore, P50 amplitude was preserved,

564   consistent with adequate fixation despite the poor visual acuity and largely excluding a macular

565   cause for the PR-VEP abnormality.

566   The photopic negative response (PhNR) component of the full-field electroretinogram is

567   severely reduced in primates treated with tetrodotoxin and in experimental models of glaucoma, in

568   keeping with a possible RGC origin (Viswanathan et al., 1999). The PhNR has also been shown to be

569   attenuated in experimental and clinical studies of glaucoma and in other forms of optic neuropathies

570   (Viswanathan et al., 1999; Gotoh et al., 2004; Sustar et al., 2009; North et al., 2010; Preiser et al.

571   2013; Machida, 2012; Morny et al., 2015). The majority of affected LHON patients in our study had

572   responses near the limits of normal, with a substantial subgroup (40%) being within normal limits.

573   There is no published data describing PhNRs in LHON, but mildly abnormal or borderline reductions

574   in the PhNR have similarly been reported in dominant optic atrophy (Miyata et al., 2004). It is

575   notable that both these mitochondrial optic neuropathies predominantly affect the papillomacular

576   bundle with relative sparing of RGC axons in the retinal periphery (Johnston et al. 1979; Kerrison et

577   al. 1995; Kjer et al. 1983; Sadun et al. 1994; Sadun et al. 2000). It should be noted that the full-field

578   PhNR provides a measure of global RGC function and it could therefore be less sensitive in detecting

579   focal RGC loss or dysfunction compared with the pattern ERG, which arises largely in central macular

580   RGCs. Other methods such as focal PhNRs, involving flash stimulation of the central macular area,

581   could potentially offer better sensitivity compared with full-field photopic negative responses, but

582   with the disadvantage of generating comparatively smaller signals. These findings are pertinent to

583   clinical trials of future therapeutic interventions, since an undetectable VEP cannot be used to

584   monitor safety and PERG could prove the objective test of choice to monitor function of the most

585   affected RGCs.

586   The international standard VEP and PERG stimuli involve high contrast checkerboard reversal

587   stimuli that are suprathreshold, whereas psychophysics enables measurement of detection

30

588 threshold. Affected LHON carriers in our study had impaired chromatic resolution in the protan and

589 deutan axes. Their achromatic spatial sensitivity was also severely compromised. Only the two least

590 affected patients (A7 and A9) were capable of performing the achromatic spatial CSF measurements,

591 but even then, steep sensitivity losses with increasing spatial frequency were evident. These findings

592 are consistent with the severe loss of the midget RGCs and the small calibre RGC axons found in post

593 mortem histological studies (Sadun et al. 1994; Kerrison et al. 1995; Sadun et al. 2000). The majority

594 of LHON patients in our study were able to detect a flickering long-wavelength light at high

595 luminance levels, but with markedly reduced temporal resolution, in keeping with a severe deficit of

596 magnocellular function. This previously unreported observation is pathologically relevant as it

597 implies that the loss of parasol RGC function is also present in acute LHON, which is consistent with

598 the LGN pathology reported in end-stage disease (Rizzo et al., 2012). Previous studies that have

599 assessed the koniocellular pathway in LHON have been limited to color vision tests (Nikoskelainen et

600 al., 1977). Only the least severely affected patients (A7 and A9) in our study were able to detect

601 flickering short-wavelength light and additional tritan deficits in the CCT tests suggested severe

602 koniocellular involvement. The smaller proportional loss found along the tritan axis compared with

603 the protan and deutan axes in the CCT test of affected LHON carriers is of doubtful clinical

604 significance, since the unusually close viewing distances adopted by 5 of the observers might have

605 selectively reduced the tritan thresholds due to rod intrusion, retinal inhomogeneities or scatter. In

606 addition, melanopsin-expressing RGCs, which are relatively preserved in LHON (Kawasaki et al.,

607 2010; La Morgia et al., 2010), are preferentially sensitive to short-wavelength light (Lucas et al.,

608 2014) and, in theory, may also contribute to blue color discrimination.

609   Previous studies on asymptomatic LHON carriers harboring the m.11778A>G mutation have

610 reported subclinical visual impairment involving both the parvocellular and the magnocellular

611 pathways as revealed by subtle chromatic and luminance contrast sensitivity deficits and impaired

612 temporal processing (Ventura et al., 2005, Sadun et al., 2006, Ventura et al., 2007, Gualtieri et al.,

613 2008, Mateus et al., 2015). Our study cohort included unaffected carriers with the m.3460A>G and

614   m.14484T>C LHON mutations, in addition to m.11778A>G. Our data indicate that all three common

615   mtDNA LHON mutations significantly impair achromatic spatial contrast sensitivity worst for higher

616   spatial frequencies. The chromatic thresholds along all three confusion lines showed mild losses

617   compared with normals highlighting dysfunction of the parvocellular pathway and confirming a

618   previous report using similar methods (Mateus et al., 2015). The majority of LHON carriers also

619   showed abnormalities of the long-wavelength temporal visual acuity, but with relatively minimal loss

620   on the L-cone TCSF measurements. These parvocelluar and magnocellular related losses were

621   present with all three common mtDNA LHON mutations. Unlike the long-wavelength sensitive

622   temporal visual acuity, impairment of the short-wavelength temporal acuity was limited to the three

623   unrelated unaffected carriers harboring the m.3460A>G mutation.

624   In conclusion, our study highlights the extent and severity of diffuse and focal

625   electrophysiological measures of RGC dysfunction in LHON. PERG abnormalities in LHON are largely

626   independent of age and can be elicited in patients with severely impaired visual acuity. Furthermore,

627   psychophysical tests of achromatic and chromatic visual function suggest severe involvement or loss

628   of midget, parasol and bistratified RGCs. These findings are highly relevant for the design of future

629   clinical trials aimed at assessing therapeutic interventions and the viability of specific RGC

630   subpopulations in patients affected with LHON.

631

636

637

638

639

640

References

1. Akiyama, H., Kashima, T., Li, D., Shimoda, Y., Mukai, R., Kishi, S., 2013. Retinal ganglion cell analysis in Leber's hereditary optic neuropathy. Ophthalmology. 120 (9), 1943-4.

2. Bach, M., Brigell, M.G., Hawlina, M., Holder, G.E., Johnson, M.A., McCulloch, D.L., Meigen, T., Viswanathan, S., 2013. ISCEV standard for clinical pattern electroretinography (PERG): 2012 update. Doc. Ophthalmol. 126, 1-7.

3. Balducci, N., Savini, G., Cascavilla, M.L., La Morgia, C., Triolo, G., Giglio, R., et al., 2015. Macular nerve fibre and ganglion cell layer changes in acute Leber's hereditary optic neuropathy. Br. J. Ophthalmol. pii: bjophthalmol-2015-307326.

4. Barboni, P., Savini, G., Valentino, M.L., Montagna, P., Cortelli, P., De Negri, A.M., et al., 2005. Retinal nerve fiber layer evaluation by optical coherence tomography in Leber's hereditary optic neuropathy. Ophthalmology. 112 (1), 120-6.

5. Barboni, P., Carbonelli, M., Savini, G., Ramos Cdo, V., Carta, A., Berezovsky, A., et al., 2010. Natural history of Leber's hereditary optic neuropathy: longitudinal analysis of the retinal nerve fiber layer by optical coherence tomography. Ophthalmology. 117 (3), 623-7.

6. Carelli, V., Rugolo, M., Sgarbi, G., Ghelli, A., Zanna, C., Baracca, A., et al., 2004a. Bioenergetics shapes cellular death pathways in Leber's hereditary optic neuropathy: a model of mitochondrial neurodegeneration. Biochim. Biophys. Acta. 1658 (1-2), 172-9.

7. Carelli, V., Ross-Cisneros, F.N., Sadun, A.A., 2004b. Mitochondrial dysfunction as a cause of optic neuropathies. Prog. Retin. Eye Res. 23 (1), 53-89.

8. Dacey, D. M., Crook, J. D., Packer, O. S., 2014. Distinct synaptic mechanisms create parallel S-ON and S-OFF color opponent pathways in the primate retina. Vis. Neurosci., 31 (Special Issue 02), 139-151.

9. Derrington, A.M., Lennie, P., 1984. Spatial and temporal contrast sensitivities of neurones in lateral geniculate nucleus of macaque. J. Physiol. 357, 219-40.

10. Dowling, J. E., 1987. The retina, an approachable part of the brain. Cambridge, Mass.: Harvard University Press.

11. Ferry, E. S., 1892. Persistence of vision. Am. J. Sci., 44(261), 192-207.

12. Gotoh, Y., Machida, S., Tazawa, Y., 2004. Selective loss of the photopic negative response in patients with optic nerve atrophy. Arch. Ophthalmol. 122(3), 341-6.

13. Gualtieri, M., Bandeira, M., Hamer, R.D., Costa, M.F., Oliveira, A.G.F., Moura, A.L.A., et al., 2008. Psychophysical analysis of contrast processing segregated into magnocellular and parvocellular systems in asymptomatic carriers of 11778 Leber's hereditary optic neuropathy. Visual Neuroscience. 25, 469–474.

14. Holder, G.E., 1987. Significance of abnormal pattern electroretinography in anterior visual pathway dysfunction. Br. J. Ophthalmol. 71(3), 166-71.

15. Holder, G.E., 2001. Pattern electroretinography (PERG) and an integrated approach to visual pathway diagnosis. Prog. Retin. Eye Res. 20 (4), 531-61.

16. Holder, G.E., 2004. Electrophysiological assessment of optic nerve disease. Eye. 18, 1133–1143.

17. Hrynchak, P.K., Spafford, M.M., 1994. Visual recovery in a patient with Leber hereditary optic neuropathy and the 14484 mutation. Optom. Vis Sci. 71 (10), 604-12.

18. Jarc-Vidmar, M., Tajnik, M., Brecelj, J., Fakin, A., Sustar, M., Naji, M., et al., 2015.Clinical and electrophysiology findings in Slovene patients with Leber hereditary optic neuropathy. Doc. Ophthalmol. 130 (3), 179-87.

685 19. Johnston, P.B., Gaster, R.N., Smith, V.C., Tripathi, R.C., 1979. A clinicopathological study of autosomal
686   dominant optic atrophy. Am. J. Ophthalmol. 88, 868–875.

687 20. Kawasaki, A., Herbst, K., Sander, B., Milea, D., 2010. Selective wavelength pupillometry in Leber
688   hereditary optic neuropathy. Clin. Experiment. Ophthalmol. 38(3), 322-4.

689 21. Kelly, D.H., 1961. Visual response to time-dependent stimuli. I. Amplitude sensitivity measurements.
690   J. Opt. Soc. Am. A. 51, 422-9.

691 22. Kerrison, J.B., Howell, N., Miller, N.R., Hirst, L., Green W.R., 1995. Leber hereditary optic neuropathy.
692   Electron microscopy and molecular genetic analysis of a case. Ophthalmology. 102, 1509–15.

693 23. Kjer,P., Jensen, O.A., Klinken, L.,1983. Histopathology of eye, optic nerve and brain in a case of
694   dominant optic atrophy. Acta Opthalmol. 61, 300–312.

695 24. Lam, B.L., Feuer, W.J., Abukhalil, F., Porciatti, V., Hauswirth, W.W., Guy, J., 2010. Leber hereditary
696   optic neuropathy gene therapy clinical trial recruitment: year 1. Arch. Ophthalmol. 128 (9),1129-35

697 25. Lam, B.L., Feuer, W.J., Schiffman, J.C., Porciatti, V., Vandenbroucke, R., Rosa, P.R., et al., 2014. Trial
698   end points and natural history in patients with G11778A Leber hereditary optic neuropathy:
699   preparation for gene therapy clinical trial. JAMA Ophthalmol. 132 (4), 428-36.

700 26. La Morgia, C., Ross-Cisneros, F.N., Sadun, A.A., Hannibal, J., Munarini, A., Mantovani, V., et al., 2010.
701   Melanopsin retinal ganglion cells are resistant to neurodegeneration in mitochondrial optic
702   neuropathies. Brain. 133 (Pt 8), 2426-38.

703 27. Lee, B.B., Martin, P.R., Grünert, U., 2010. Retinal connectivity and primate vision. Progress in Retinal
704   and Eye Research, 29(6), 622-639.

705 28. Lenassi, E., Robson, A.G., Hawlina, M., Holder, G.E., 2012. The value of two field PERG in routine
706   clinical electrophysiological practice. Retina. 32(3), 588-99.

707 29. Lennie, P., Movshon, J. A., 2005. Coding of color and form in the geniculostriate visual pathway. J.
708   Opt. Soc. Am. A. Opt. Image Sci. Vis., 10(10), 2013-2033.

709 30. Levin, L.A., 2015. Superoxide generation explains common features of optic neuropathies associated
710   with cecocentral scotomas. J. Neuro-Ophthalmol. 35, 152-1.

711 31. Lin, C.S., Sharpley, M.S., Fan, W., Waymire, K.G., Sadun. A.A., Carelli, V., et al., 2012. Mouse mtDNA
712   mutant model of Leber hereditary optic neuropathy. Proc. Natl. Acad. Sci. U.S.A. 109 (49), 20065-70.

713 32. Lucas, R.J., Peirson, S.N., Berson, D.M., Brown, T.M., Cooper, H.M., Czeisler, C.A., et al., 2014.
714   Measuring and using light in the melanopsin age. Trends Neurosci. 2014, 37(1):1-9.

715 33. Mackey, D.A., Oostra, R.J., Rosenberg, T., Nikoskelainen, E., Bronte-Stewart, J., Poulton, J., et al.,
716   1996. Primary pathogenic mtDNA mutations in multigeneration pedigrees with Leber hereditary
717   optic neuropathy. Am. J. Hum. Genet. 59 (2), 481-5.

718 34. Machida, S., 2012. Clinical applications of the photopic negative response to optic nerve and retinal
719   diseases. J. Ophthalmol. 2012, 397178.

720 35. Majander, A., Bitner-Glindzicz, M., Chan, C.M., Duncan, H.J., Chinnery, P.F., Subash, M., et al., 2016.
721   Lamination of the outer plexiform layer in optic atrophy caused by dominant WFS1 mutations.
722   Ophthalmology. pii: S0161-6420(16)00026-9. doi: 10.1016/j.ophtha.2016.01.007.

723 36. Mashima, Y., Imamura, Y., Oguchi, Y., 1997. Dissociation of damage to spatial and luminance
724   channels in early Leber's hereditary optic neuropathy manifested by the visual evoked potential. Eye
725   (Lond). 11 (Pt 5), 707-12.

726 37. Mateus, C., d'Almeida, O.C., Reis, A., Silva, E., Castelo-Branco, M., 2015. Genetically induced
727   impairment of retinal ganglion cells at the axonal level is linked to extrastriate cortical plasticity.
728   Brain Struct. Funct. DOI 10.1007/s00429-015-1002-2.

729 38. Miyata, K., Nakamura, M., Kondo, M., Lin, J., Ueno, S., Miyake, Y., Terasaki, H., 2007. Reduction of
730 oscillatory potentials and photopic negative response in patients with autosomal dominant optic
731 atrophy with OPA1 mutations. Invest. Ophthalmol. Vis. Sci. 48(2), 820-4.

732 39. Mizoguchi, A., Hashimoto, Y., Shinmei, Y., Nozaki, M., Ishijima, K., Tagawa, Y., Ishida, S., 2015.
733 Macular thickness changes in a patient with Leber's hereditary optic neuropathy. BMC Ophthalmol.
734 18, 15:27.

735 40. Morny, E.K., Margrain, T.H., Binns, A.M., Votruba, M., 2015. Electrophysiological ON and OFF
736 Responses in Autosomal Dominant Optic Atrophy. Invest. Ophthalmol. Vis. Sci. 56 (13), 7629-37.

737 41. Nikoskelainen, E., Sogg, R.L., Rosenthal, A.R., Friberg, T.R., Dorfman, L.J., 1977. The early phase in
738 Leber hereditary optic atrophy. Arch. Ophthalmol. 95 (6), 969-78

739 42. Nikoskelainen, E., Hoyt, W.F., Nummelin, K., 1982. Ophthalmoscopic findings in Leber's hereditary
740 optic neuropathy. I. Fundus findings in asymptomatic family members. Arch. Ophthalmol. 100,
741 1597–602.

742 43. Nikoskelainen, E.K., Huoponen, K., Juvonen, V., Lamminen, T., Nummelin, K., Savontaus, M.L., 1996.
743 Ophthalmologic findings in Leber hereditary optic neuropathy, with special reference to mtDNA
744 mutations. Ophthalmology. 103, 504-14.

745 44. North, R.V., Jones, A.L., Drasdo, N., Wild, J.M., Morgan, J.E., 2010. Electrophysiological evidence of
746 early functional damage in glaucoma and ocular hypertension. Invest. Ophthalmol. Vis. Sci. 51(2),
747 1216-22.

748 45. Odom, J.V., Bach, M., Brigell, M., Holder, G.E., McCulloch, D.L., Tormene, A.P., Vaegan, 2010. ISCEV
749 standard for clinical visual evoked potentials (2009 update). Doc. Ophthalmol. 120, 111–9.

750 46. Paramei, G.V., Oakley, B., 2014. Variation of color discrimination across the life span. J. Opt. Soc. Am.
751 A. Opt. Image Sci. Vis. 31, A375-84.

752 47. Porter, T. C., 1902. Contributions to the study of flicker. Paper II. Proceedings of the Royal Society of
753 London. Series A, 70, 313-329.

754 48. Preiser, D., Lagrèze, W.A., Bach, M., Poloschek, C.M., 2013. Photopic negative response versus
755 pattern electroretinogram in early glaucoma. Invest. Ophthalmol. Vis. Sci. 54(2), 1182-91.

756 49. Ripamonti, C., Henning, G.B., Ali, R.R., Bainbridge, J.W., Robbie, S.J., Sundaram, V., et al., 2014.
757 Nature of the visual loss in observers with Leber's congenital amaurosis caused by specific mutations
758 in RPE65. Invest. Ophthalmol. Vis. Sci. 55, 6817-28.

759 50. Robson, J. G., 1966. Spatial and temporal contrast sensitivity functions of the visual system. Journal
760 of the Optical Society of America, 56, 1141-1142.

761 51. Rodieck, R. W., 1998. The First Steps in Seeing. Sunderland, Mass.: Sinauer.

762 52. Ryan, S., Arden, G.B., 1988. Electrophysiological discrimination between retinal and optic nerve
763 disorders. Doc. Ophthalmol. 68(3-4), 247-55.

764 53. Sadun, A.A., Kashima, Y., Wurdeman, A.E., Dao, J., Heller, K., Sherman, J., 1994. Morphological
765 findings in the visual system in a case of Leber's hereditary optic neuropathy. Clin. Neurosci. 2, 165–
766 172.

767 54. Sadun, A.A., Win, P.H., Ross-Cisneros, F.N., Walker, S.O., Carelli, V, 2000. Hereditary optic
768 neuropathy differentially affects smaller axons in the optic nerve. Tr. Am. Ophth. Soc. 98, 223-35.

769 55. Sadun, A.A., Salomao, S.R., Berezovsky, A., Sadun, F., Denegri, A.M., Quiros, P.A., et al., 2006.
770 Subclinical carriers and conversions in Leber hereditary optic neuropathy: a prospective
771 psychophysical study. Trans. Am. Ophthalmol. Soc. 104, 51-61.

772 56. Sadun, A.A., Karanjia, R., Pan, B.X., Ross-Cisneros, F.N., Carelli, V., 2015. Reactive oxygen species in
773 mitochondrial optic neuropathies: Comment. J. Neuro-Ophthalmol. 35, 445-6.

774 57. Sharkawi, E., Oleszczuk, J.D., Holder, G.E., Raina, J., 2012. Clinical and electrophysiological recovery
775   in Leber hereditary optic neuropathy with G3460A mutation. Doc. Ophthalmol. 125 (1), 71-4.

776 58. Stockman, A., Plummer, D.J., 1998. Color from invisible flicker: a failure of the Talbot-Plateau law
777   caused by an early 'hard' saturating nonlinearity used to partition the human short-wave cone
778   pathway. Vision Res. 38, 3703-28.

779 59. Stockman, A., Plummer, D.J., Montag, E.D., 2005. Spectrally opponent inputs to the human
780   luminance pathway: slow +M and -L cone inputs revealed by intense long-wavelength adaptation. J.
781   Physiol. 566, 61-76.

782 60. Stockman, A., Henning, G.B., Michaelides, M., Moore, A.T., Webster, A.R., Cammack, J., Ripamonti,
783   C., 2014a. Cone dystrophy with "supernormal" rod ERG: psychophysical testing shows comparable
784   rod and cone temporal sensitivity losses with no gain in rod function. Invest. Ophthalmol. Vis. Sci. 55,
785   832-40.

786 61. Stockman, A., Henning, G.B., Moore, A.T., Webster, A.R., Michaelides, M., Ripamonti, C., 2014b.
787   Visual consequences of molecular changes in the guanylate cyclase-activating protein. Invest.
788   Ophthalmol. Vis. Sci. 55, 1930-40.

789 62. Sustar, M., Cvenkel, B., Brecelj, J., 2009. The effect of broadband and monochromatic stimuli on the
790   photopic negative response of the electroretinogram in normal subjects and in open-angle glaucoma
791   patients. Doc. Ophthalmol. 118(3), 167-77.

792 63. van Nes, F. L., Bouman, M. A., 1967. Spatial modulation transfer in the human eye. J. Opt. Soc. Am.,
793   57, 401-406.

794 64. Ventura, D.F., Quiros, P., Carelli, V., Salomão, S.R., Gualtieri, M., Oliveira, A.F.G., et al., 2005.
795   Chromatic and luminance contrast sensitivities in asymptomatic carriers from a large Brazilian
796   pedigree of 11778 Leber Hereditary Optic Neuropathy. Invest. Ophthalmol. Vis. Sci. 46, 4809–4814.

797 65. Ventura, D.F., Gualtieri, M., Oliveira, A.G., Costa, M.F., Quiros, P., Sadun, F., et al., 2007. Male
798   prevalence of acquired color vision defects in asymptomatic carriers of Leber's hereditary optic
799   neuropathy. Invest. Ophthalmol. Vis. Sci. 48 (5), 2362-70.

800 66. Viswanathan, S., Frishman, L.J., Robson, J.G., Harwerth, R.S., Smith, E.L. 3rd, 1999. The photopic
801   negative response of the macaque electroretinogram: reduction by experimental glaucoma. Invest.
802   Ophthalmol. Vis. Sci. 40(6), 1124-36.

803 67. Viswanathan. S., Frishman, L.J., Robson, J.G., 2000. The uniform field and pattern ERG in macaques
804   with experimental glaucoma: removal of spiking activity. Invest. Ophthalmol. Vis. Sci. 41(9):2797-
805   810.

806 68. Wandell, B.A., 1995. Foundations of Vision. Sutherland, Massashusets: Sinauer Associates, Inc. 111-
807   152.

808 69. Watson, A.B. 2014. A formula for human retinal ganglion cell receptive field density as a function of
809   visual field location. J. Vis. 14, 15.1–17.

810 70. Wässle, H., Boycott, B. B., 1991. Functional architecture of the mammalian retina. Physiol. Rev.,
811   71(2), 447-480.

812 71. Zhang, Y., Huang, H., Wei, S., Qiu, H., Gong, Y., Li, H., et al., 2014. Characterization of retinal nerve
813   fiber layer thickness changes associated with Leber's hereditary optic neuropathy by optical
814   coherence tomography. Exp. Ther. Med. 7(2), 483-7.

815 72. Ziccardi, L., Sadun, F., De Negri, A.M., Barboni, P., Savini, G., Borrelli, E., et al., 2013. Retinal function
816   and neural conduction along the visual pathways in affected and unaffected carriers with Leber's
817   hereditary optic neuropathy. Invest. Ophthalmol. Vis. Sci. 54 (10), 6893-901.

818 73. Ziccardi, L., Parisi,V., Giannini,D., Sadun, F., De Negri, A.M., Barboni, P., et al., 2015. Multifocal VEP
819   provide electrophysiological evidence of predominant dysfunction of the optic nerve fibers derived
820   from the central retina in Leber's hereditary optic neuropathy. Graefes Arch. Clin. Exp. Ophthalmol.
821   253, 1591–1600.

822 74. Yu-Wai-Man, P., Chinnery, P.F., 2013. Leber Hereditary Optic Neuropathy. In: Pagon RA, Adam MP,
823   Ardinger HH, Wallace SE, Amemiya A, Bean LJH, Bird TD, Fong CT, Mefford HC, Smith RJH, Stephens
824   K, editors. GeneReviews® [Internet]. Seattle (WA): University of Washington, Seattle; 1993-2016.
825   2000 Oct 26 [updated 2013 Sep 19].

826 75. Yu-Wai-Man, P., Votruba, M., Moore, A.T., Chinnery, P.F, 2014. Treatment strategies for inherited
827   optic neuropathies – Past, present and future. Eye, 28(5), 521-37.

828

829

Supplementary data

Table S1. Results of the macular and optic nerve head optical coherence tomography imaging.

Retinal layer	Layer thickness (µm) (mean±SD)			
	Affected LHON (n=26 eyes)	P *	Unaffected LHON (n=18 eyes)	Control (n=48 eyes)
Macula				
Retina	306.3 ± 24.8	<0.001	349.0± 8.5	340.8 ± 13.3
RNFL	19.2 ± 2.8	<0.001	24.8 ± 1.1	24.2 ± 2.1
GCL-IPL	47.1 ± 14.6	<0.001	94.9 ± 3.4	93.5 ± 7.8
INL	45.1 ± 4.7	<0.001	39.2 ± 2.3	39.6 ± 3.5
OPL	33.0 ± 8.2	0.955	34.9 ± 4.7	32.3 ± 4.0
OPL-ONL	110.9 ± 10.0	<0.001	107.4 ± 8.1	102.0 ± 8.6
Outer retina	83.9 ± 3.4	0.002	82.9 ± 2.6	81.5 ± 2.7
Peripapillary RNFL				
Inferotemporal	83.2 ± 47.3		152.4 ± 18.6	147**
Temporal	33.4 ± 17.2		72.7 ± 2.5	78**
Superotemporal	73.5 ± 46.0		122.3 ± 20.4	138**
Superonasal	77.1 ± 35.2		111.4 ± 30.8	102**
Nasal	54.0 ± 21.1		83.3 ± 13.7	72**
Inferonasal	79.7 ± 35.0		126.4 ± 26.4	108**
Average	66.8 ± 30.0		111.4 ± 12.4	108**

Abbreviations: GCL-IPL, ganglion cell layer - inner plexiform layer complex; INL, inner nuclear layer; LHON, Leber hereditary optic neuropathy; OPL, outer plexiform layer; OPL-ONL, outer plexiform layer - outer nuclear layer complex; RNFL, retinal nerve fiber layer.

* Mann-Whitney *U* Test
** Heidelberg OCT normative mean

Table S2. L-cone critical flicker fusion variables.

Observer	L-cone				
	The lowest radiance (log$_{10}$ quanta s^{-1}deg^{-2})	Ferry-Porter slope Per decade	R^2	Frequency (Hz) at 8.5 log$_{10}$ quanta s^{-1}deg^{-2} radiance	Plateau frequency (Hz) at 10.3-10.6 log$_{10}$ quanta s^{-1}deg^{-2} radiance
Normal mean±SE	6.65±0.06	9.16±0.35	0.998	27.90±0.91	40.18±0.88
LHON					
A1	10.00	0.295	0.017	ND	11.60
A2	8.99	2.873	0.933	ND	13.00
A3	9.71	4.594	0.931	ND	6.78
A4	10.63	ND	ND	ND	8.92
A6	10.37	ND	ND	ND	16.00
A7	8.05	2.914	0.762	ND	19.67
A9	8.45	10.847	0.896	ND	21.84
A10	10.94	ND	ND	ND	0.67
A11					
LHON mean±SE	9.64±0.43	4.30±1.59	0.71±0.18		12.31±2.84
Mann-Whitney *U* test, p	<0.001	<0.001			<0.001
Carrier					
U1	6.89	8.62	0.99	26.08	41.89
U2	7.46	5.37	0.97	19.32	29.11
U3	7.21	7.85	0.99	17.02	33.17
U4	5.42	9.24	0.92	24.13	37.22
U5	7.21	8.20	0.94	21.34	34.80
U6	7.16	6.55	0.93	18.83	30.72
U7	7.43	9.30	0.99	19.07	28.89
U8	6.84	8.00	0.99	27.21	39.56
U9	7.18	7.17	0.95	19.48	32.89
All carriers Mean±SE	6.98±0.19	7.81±0.43	0.96±0.01	21.39±1.19	34.25±1.43
Mann-Whitney *U* test, p	0.004	0.035*		0.001*	0.004*

Abbreviation: LHON, Leber hereditary optic neuropathy; ND, not determined.

844 **Table S3. S-cone critical flicker fusion variables.**

Observer	S-cone				
	The lowest radiance ($\log_{10}$ quanta $s^{-1}deg^{-2}$)	Ferry-Porter slope		Frequency (Hz) at 8.5 $\log_{10}$ quanta $s^{-1}deg^{-2}$ radiance	Plateau frequency (Hz) at 9.2-9.4 $\log_{10}$ quanta $s^{-1}deg^{-2}$ radiance
		Per decade	R^2		
Normal	6.77±0.09	7.28±0.29	0.998	18.99±0.89	23.88±0.98
Affected LHON					
A7	8.13	2.20	0.8219	ND	10.44
A9	8.14	0.1074	0.055	ND	7.63
All affected	8.14±0.00	4.30±1.59			9.04±0.53
Unaffected					
U1	7.44	10.12	0.99	20.50	26.50
U2	7.11	7.27	0.91	18.80	22.25
U3	9.31	2.57	0.70	1.06	3.39
U4	7.05	9.66	0.95	16.07	22.17
U5	7.18	6.14	0.98	17.15	22.33
U6	6.89	6.30	0.94	17.93	21.11
U7	7.44	6.97	0.98	14.62	18.33
U8	7.42	5.64	0.98	10.33	16.11
U9 TC	6.91	6.39	0.91	15.86	23.28
All unaffected	7.42±0.23	6.78±0.74	0.95±0.01	14.70±1.95	19.50±2.11
Mann-Whitney U test, p	0.001*	0.411		0.055	0.049

845 Abbreviation: LHON, Leber hereditary optic neuropathy; ND, not determined.

846

847

848
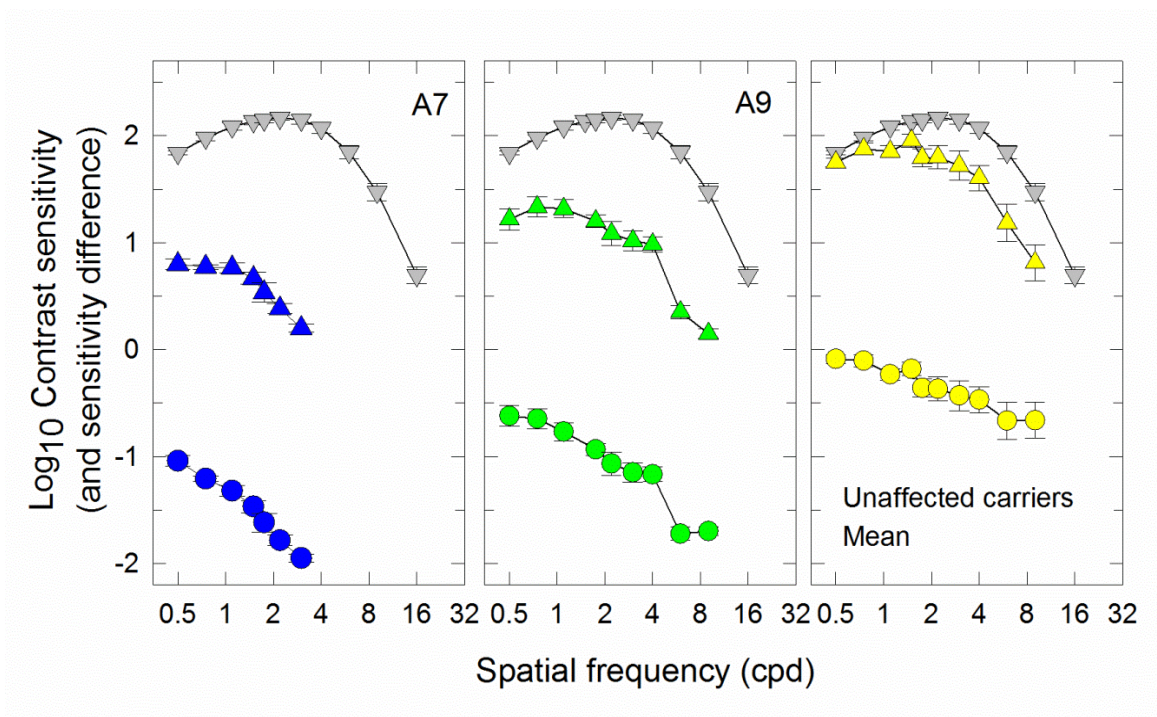
Figure S1. Achromatic spatial contrast sensitivity functions. CSFs expressed as $\log_{10}$ sensitivity as a function of spatial frequency (cycles per degree, cpd – logarithmic scale) are shown for two affected LHON carriers (A7, A9) (blue triangles), for the mean of the 9 unaffected LHON carriers (yellow triangles) and for normal controls (inverted grey triangles). The difference in sensitivity between LHON carriers and normal is also indicated in each panel by colored circles. The symbols and error bars represent the mean ± 1 SEM across normal observers, repeated runs of individual LHON patients or across 9 unaffected LHON carriers.

856